Biophysical Chemistry 40 (1991) 197–205
Elsevier Science Publishers B.V., Amsterdam

BIOCHE 01569

The effects of lithium, rubidium, cesium and magnesium ions on the close packing of persistence-length DNA fragments

S. Trohalaki *, H.L. Frisch and L.S. Lerman **

Center for Biological Macromolecules and the Departments of Chemistry and Biological Sciences, State University of New York at Albany, Albany, New York, NY 12222, USA

Received 25 September 1990
Accepted 10 December 1990

DNA packing; Osmotic pressure; Clustering function; Scaled particle theory; MgDNA

By application of scaled particle theory to persistence-length DNA fragments in sedimentation-equilibrium at speeds high enough to maintain close packing, the range of interhelical electrostatic repulsion was evaluated with LiCl, RbCl, CsCl, and $MgCl_2$ as supporting electrolytes. Analysis of the data in terms of the Zimm cluster function confirmed that the net interaction between helices is purely repulsive in all cases. At constant ionic strength the electrostatic radius of the rod-like DNA decreases as the counterion changes from Li^+ to Rb^+ to Cs^+. In contrast to univalent counterions, electrostatic radius increases with Mg^{2+} concentration, except at very low (mM) $MgCl_2$ concentrations. All solutions undergo a reversible transition to a turbid, optically anisotropic phase at a slightly salt-dependent, critical DNA concentration, as observed previously for NaDNA.

1. Introduction

We have examined the sedimentation-equilibrium distribution of persistence-length DNA fragments at centrifugal field strengths that effect close approach of helices, where the interhelical separation is comparable with that of procaryotic intracellular densities and intraviral packing. Previously [1] we have shown that the relationship between osmotic pressure and DNA concentration in dense NaDNA solutions departs radically from ideal-solution behavior. The properties of similarly dense solutions of longer DNA molecules were also found [2] to correspond to an extension of the theory, where the molecules are treated as a slightly flexible concatenation of rods. Interactions between helices were found to be purely repulsive and, at sufficient ionic strength, they were satisfactorily simplified as a hard-core potential. The solution properties were found to agree closely with scaled particle theory (SPT) [3] extended to spherocylinders [4] with a fitting parameter representing the hard-core radius. This radius is a sum of two contributions—the Van der Waals radius of the rod-like helix plus the shielded electrostatic repulsion between rods. A phase transition takes place when the DNA volume fraction exceeds a particular salt-dependent limit, resulting in a denser, ordered phase in equilibrium with the isotropic solution.

The effect of univalent counterions differing in ionic radius (Li^+, Rb^+, and Cs^+) and of a divalent counterion (Mg^{2+}) on electrostatic repulsion and on the ordering transition is reported here. The relevance of counterion size has been addressed in the context of counterion condensation theory [5–8]. Recent investigations [9–11] have sup-

* To whom correspondence should be addressed at the Department of Chemical Engineering and Materials Science, Syracuse University, Syracuse, New York, NY, 13244, USA.
** Present address: Department of Biology, Massachusetts Institute of Technology, Cambridge, MA 02139, USA.

0301-4622/91/$03.50

plied evidence for and against the formation of gels and aggregates by short DNA fragments in the presence of univalent and divalent cations. There has also been recent evidence of a hydration force between parallel DNA helices approaching contact [12]. Because each counterion used here differs in hydration number, the relevance of hydration force in this system can be examined.

2. Materials and methods

Persistence-length DNA fragments were prepared by two methods. In the first, chicken erythrocyte DNA was dialyzed against 10 m*M* NaCl, 10 m*M* Tris–Cl, pH 8.0, and 10 m*M* Na-EDTA, pH 8.0, diluted with two volumes of glycerol, and then sheared at a volume of 400 ml in a dry ice–ethanol bath using a VirTis 60K rotating blade homogenizer (Virtis Co., Gardiner, NY, USA) at 50,000 rpm for 1 hour. Even at this high rate of shear the presence of small but significant fractions of molecules up to 500 base pairs were detected by gel electrophoresis. Length fractionation employing poly(ethylene oxide)-induced precipitation [13] resulted in an acceptable, homogeneous fraction. Agarose gel electrophoresis using size markers from a *Hae*III digest of ϕxi74 DNA showed that the mass distribution lay between the 72 and 318 base-pair markers. Alternatively, DNA was sheared in smaller, 150 ml shearing flasks at dry ice–acetone temperature.

The final dialysis of samples for ultracentrifugation at DNA concentrations of 65–100 mg/ml was carried out as previously described [1] at 4°C for $MgCl_2$ dialysates and at 20°C for all others. The aqueous dialyzing solutions containing $MgCl_2$ at concentrations of 1.00 *M*, 0.500 *M*, 0.100 *M*, 15.0 m*M*, 10.0 m*M*, and 1.0 m*M* also contained 1 m*M* Na-cacodylate, pH 8.0, and 1 m*M* Tris–Cl, pH 8.0. The 0.200 *M* LiCl and 0.200 *M* RbCl dialyzing solutions also contained 0.1 m*M* Na-EDTA, pH 8.0 and 1 mM Tris–Cl, pH 8.0, as did the solutions containing CsCl at concentrations of 1.50 *M*, 1.00 *M*, 0.500 *M* and 0.200 *M*.

Samples were equilibrated in the centrifuge described by Brian et al. [1]. Each cell contained about 7 μl of solution and 0.5 μl of poly(trifluorochloroethylene) (FC-43; 3M Co., West Caldwell, NJ, USA). The extremely short optical path, 0.1 mm, was measured by its interference pattern as previously described [1]. UV scanning was carried out at 302 nm. The approach to equilibrium after each speed increment required 5–7 days in the centrifuge and was deemed adequate when scans taken at 48-hour intervals agreed to within 1% of the full-scale concentrations. The equilibrium state was the same whether it was approached from a higher or a lower speed.

Table 1

Density increments

$[MgCl_2]$ [a]	$\left(\frac{\partial\rho}{\partial c_2}\right)_\mu$ [b]	$\left(\frac{\partial\rho}{\partial c_2}\right)_{\mu,\mathrm{fit}}$ [c]
1.000 *M*	0.494	0.502
0.500 *M*	0.530	0.526
0.100 *M*	0.602	0.590
15.0 m*M*	–	0.675
10.0 m*M*	0.684	0.694
1.0 m*M*	0.820	0.818

[a] Concentration of the dialysate.
[b] Experimental values of the density increment.
[c] Values of the density increment obtained from a linear least-squares fit of the experimental values as a function of $MgCl_2$ concentration.

Density increments were determined for DNA dialyzed against the specified $MgCl_2$ concentrations using a standard procedure for pycnometry [14] and are presented in Table 1. Previously published values [15] were used for all other samples.

3. Results and discussion

3.1 DNA and magnesium ion

The reduced osmotic pressure as a function of DNA concentration, c_2, for samples dialyzed against 1 m*M*–1 *M* $MgCl_2$ is shown in Fig. 1. The function was calculated from the sedimentation-equilibrium distribution by means of the Eisenberg relation [1] up to the onset of the ordering transition (except for the 10 m*M* $MgCl_2$ dialysate, in which partial overflow into the reference sector obscured the transition). The 0.1 *M*, 0.5 *M*, and

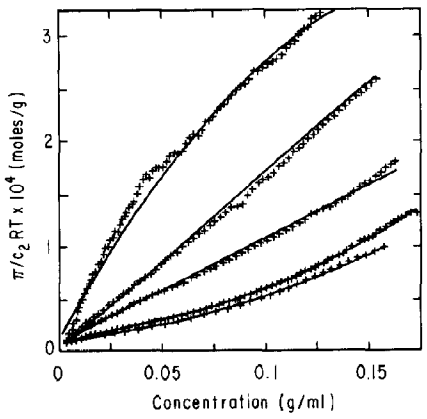

Fig. 1. Reduced osmotic pressure as a function of DNA concentration for (clockwise) 1 mM, 10 mM, 15 mM, 0.1 M, and 1.0 M $MgCl_2$ dialysates (the 0.5 M $MgCl_2$ function was omitted for clarity). Experimental points are indicated by (+) and the solid curves were drawn according to SPT for the 0.1 M and 1.0 M $MgCl_2$ functions or according to the virial equation for the 1 mM, 10 mM, and 15 mM $MgCl_2$ functions, as indicated in the text.

1.0 M $MgCl_2$ functions are similar in appearance: pronounced upward curvature indicates significant contributions from many-body interactions [16]. In this range of $MgCl_2$ concentration, 0.1 M and above in the dialysate, the degree of upward curvature increases slightly with increasing salt concentration, opposite to the effect seen with singly charged cations. The functions found for samples equilibrated with 10 mM and 15 mM $MgCl_2$ appear as straight lines, suggesting that many-body interactions are compensated by other effects. A slight downward curvature is seen for the 1 mM $MgCl_2$ function, indicating that the effective third virial coefficient is small and negative.

The Zimm clustering function, shown in Fig. 2 for the 0.1 M and the 15 mM $MgCl_2$ dialysates, decreases monotonically, showing that the net interhelical forces are exclusively repulsive. Exclusively repulsive interactions are found at all other $MgCl_2$ concentrations as well. This result is inconsistent with the suggestion by Mandelkern et al. [11] that rodlike DNA molecules aggregate into bundles of about seven parallel helices; a role for divalent ions is implied by abolition of the effect by EDTA. Later studies [9,10] of the effect of Mg^{2+} on association of short DNA fragments argue against side-by-side aggregation of short rod-like DNA.

An equation of state derived from SPT [3], which gives the pressure P for an isotropic fluid containing hard spherocylinders at number density ρ [4] is a function of particle length l and radius a:

$$\frac{P}{\rho kT} = \frac{1 + B + C + D + (B + C)^2 + \frac{1}{3}D(B + \frac{3}{2}C)}{(1 - B - C)^3}, \quad (1)$$

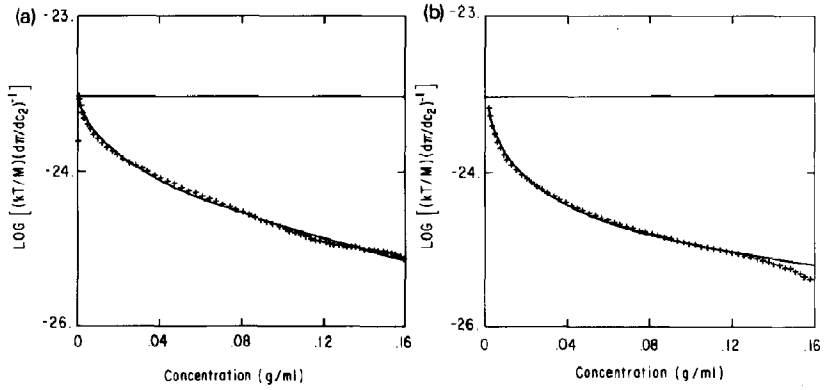

Fig. 2. Log of the clustering function versus DNA concentration for (a) the 0.1 M $MgCl_2$ dialysate, and (b) for the 15 mM $MgCl_2$ dialysate. Points (+) were calculated from the experimental data and the solid curves were drawn according to SPT.

where $B = a^2 l\rho$, $C = \frac{4}{3}a^3\rho$, $D = \frac{1}{2}al^2\rho$, k is Boltzmann's constant and T the temperature (K). In fitting the theoretical function to the experimental reduced osmotic pressure, l and a were adjusted independently to a minimal χ^2 while maintaining the relationship for B-DNA between length and molecular weight M_2:

$$l = 3.4 \cdot 10^{-8}\left(\frac{M_2}{M_{bp}}\right) \text{ cm}, \quad (2)$$

where M_{bp} is the average molar mass of one base pair.

As shown in Fig. 1 there is close correspondence between the SPT equation of state and the reduced osmotic pressure for the 1.0 M and the 0.1 M $MgCl_2$ dialysates (as well as for the 0.5 M $MgCl_2$ dialysate, not shown). The best SPT fit to the 1 mM $MgCl_2$ function (not shown) is poor in that it displays considerable upward curvature. The 10 mM and 15 mM functions are fitted very well by straight lines (with correlation coefficient of 0.998 and 0.999, respectively), indicating that the third virial coefficients are effectively zero. The 1 mM $MgCl_2$ function requires a quadratic function for a good fit (the molecular weight was adjusted independently to a minimal χ^2 with the third virial coefficient appearing negative but small in magnitude). Accordingly, a suitable equation of state is the virial expansion of Π/c_2RT (where R denotes the gas constant) taken to first order for the 10 mM and 15 mM $MgCl_2$ dialysate:

$$\frac{\Pi}{c_2RT} = \frac{1}{M_2} + B_2c_2 + B_3c_2, \quad (3)$$

where B_2 is the second virial coefficient and the third virial coefficient, B_3, is set to zero in the cases of 10 mM and 15 mM $MgCl_2$. Correspondence between eq. (3) and the data is presented in Fig. 1.

The failure of SPT indicates that the interactions at low salt are characterized by a soft potential; the hard-core approximation does not hold for higher-order interactions and SPT fails as is expected theoretically for low ionic strength [17]. The second virial coefficient for a soft potential can, as shown by Onsager [17], be represented by a hard-core radius for binary interactions only, not those of higher order.

An approximation for long cylinders of constant radius found by Zimm [16] relates the second virial coefficient to the radius:

$$B_2 = \frac{\pi N_{Av} a l^2}{2M_2}, \quad (4)$$

where N_{Av} is Avagadro's number. Substituting eq. (2) into eq. (4) and using the second virial coefficients obtained from the fits of eq. (3) to the data, radii representative of binary interactions were obtained for low salt (1–15 mM $MgCl_2$) samples.

Table 2

Effective radii, molecular weights, asymmetry ratios, and critical parameters for $MgCl_2$ dialysates and effective radii for NaCl dialysates

[Salt] [a]	M_2 [b] ($\times 10^5$ g mol^{-1})	a_{Mg} [c] (Å)	a_{Na} [d] (Å)	l/a_{Mg} [e]	$(\Pi/c_2RT)_{crit}$ ($\times 10^4$ mol g^{-1})	c_{crit} (g ml^{-1})	ϕ_{crit}
1.0 mM	0.640	128	180*	4.66	3.56	0.151	37.3
10.0 mM	3.11	61.5	75.9*	28.9	–	–	–
15.0 mM	1.26	37.6	65.1*	19.8	1.79	0.161	2.46
0.100 M	1.54	10.5	31.9*	79.2	0.956	0.160	0.180
0.500 M	1.86	10.7	17.4*	93.7	0.990	0.159	0.186
1.000 M	1.22	11.0	13.0	60.3	1.30	0.177	0.220

[a] Dialysate salt concentration.
[b] Molecular weight of MgDNA.
[c] Effective radii of MgDNA.
[d] Effective radii for NaDNA taken or extrapolated (*) from Brian et al. [1].
[e] Asymmetry ratio for MgDNA.

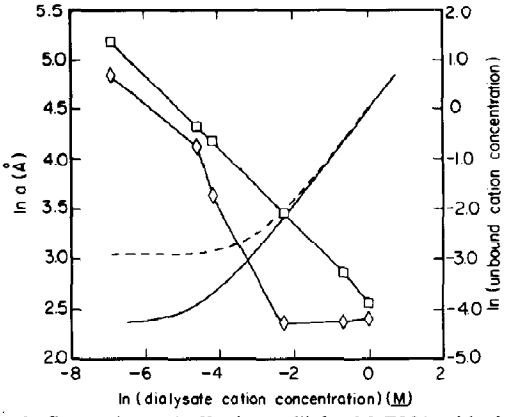

Fig. 3. Comparison of effective radii for MgDNA with those for NaDNA. Corresponding to the left-hand abcissa, ln radius (◇ for magnesium, □ for sodium) is plotted as a function of the natural logarithm of the cation concentration in the dialysate. Also, corresponding to the right-hand abcissa, the ln of the total cation concentration in the DNA solution is drawn for magnesium (solid line) and for sodium (dashed line) according to Donnan-equilibrium calculations described in the text.

These radii together with the effective radii obtained from the fits by SPT to the high salt (0.1–1.0 *M* $MgCl_2$) data are presented in Table 2. Values for effective radii found in the presence of Na^+, or values extrapolated from that data, are included for comparison in Table 2. The smallest radius seen (10.5 Å), corresponding to the 0.1 *M* $MgCl_2$ dialysate, is only one-third the radius extrapolated for 0.1 *M* NaCl (31.9 Å) and is even smaller than the radius corresponding to the 2.0 *M* NaCl dialysate (11.7 Å). It is close to the mean Van der Waals radius of the B-DNA helix. The MgDNA effective radii are compared to the NaDNA radii in Fig. 3, which also compares the concentrations of the two unbound cations in the DNA solution. These concentrations were calculated from Donnan equilibrium where the uncompensated phosphate charge fraction was assumed to be 24% for Na^+ and 12% for Mg^{2+}, as predicted by Manning [6]. It will be seen in Fig. 3 that at high cation concentration the unbound cation concentration is equal to the dialysate and at low concentration approaches phosphate equivalence. It will also be seen that there is a strikingly different dependence of the radius on free cation concentration at high concentrations such that decreasing magnesium leaves the radius almost unchanged (actually a little smaller) while decreasing sodium results in a rapid increase in the effective radius. In this range of concentration, the Donnan correction to the dialysate is negligible.

Values for the molecular weight are also included in Table 2: The values for the 1 m*M*, 10 m*M*, and 15 m*M* $MgCl_2$ dialysates were calculated from the *y*-intercept of the quadratic and linear least-squares fits to the data; but, because eq. (4) is independent of molecular weight, they do not affect the effective radii as computed. The molecular weight for the 15 m*M* sample agrees with the average found from gel electrophoresis: The value for the 1 m*M* sample is low but is not unreasonable (theory predicts that particles of larger axial ratios will segregate into the anisotropic phase) [18–21] and the 10 m*M* value is about twice the average determined from gel electrophoresis. The molecular weights reported for the 0.1 *M*, 0.5 *M*, and 1.0 *M* $MgCl_2$ samples taken from the two-parameter fit of SPT are $1.54 \cdot 10^5$, $1.86 \cdot 10^5$, and $1.22 \cdot 10^5$ g mol^{-1} respectively. They are in good agreement with the result from gel electrophoresis.

In the range of 0.1–1.0 *M* $MgCl_2$, radius increases with increasing magnesium concentration, opposite to what is expected from greater charge screening at higher salt. The trend is small but not insignificant. It is consistent with the spacings between helices found in DNA fibers formed in the presence of poly(ethylene oxide) (PEO) and $MgCl_2$ [22], where PEO induces DNA condensation by an excluded volume effect [23]. Lerman and Wang (unpublished data) have observed that at PEO concentrations less than 200 mg/ml condensation takes place at lower PEO concentration in solutions equilibrated with 0.1 *M* $MgCl_2$ than at either higher or lower magnesium concentrations. This magnesium concentration matches that giving the minimum effective radius reported here and suggests a minimum in the repulsive potential between DNA molecules as a function of Mg^{2+} concentration. The radii in the range of 1–15 m*M* $MgCl_2$ are much larger than those found at higher salt and diminish with increasing salt concentration, similar to the effect of singly charged cations. This trend is pronounced and consistent with

greater charge screening at higher salt concentration. A plausible explanation for these combined results is that adjacent helices share common Mg^{2+} ions thereby forming interhelical bridges allowing closer approach and resulting in a smaller average effective radius. As $MgCl_2$ concentration increases, the number of shared Mg^{2+} ions decreases and bridging occurs to a lesser extent due to competition of separate Mg^{2+} ions binding to each helix, resulting in an increase in hard-core radius. At very low $MgCl_2$ concentrations the helices are much too far apart to share common Mg^{2+} ions. Interhelical bridging by Mg^{2+} is also consistent with the results of Auer et al. [22], where interhelical spacing of DNA condensed in the presence of PEO and $MgCl_2$ decreases slightly as magnesium concentration decreases from 0.1 to 0.02 *M*. Fried and Bloomfield [9] have presented evidence for Mg^{2+} bridges between 200 base-pair DNA fragments for DNA concentrations of 5–76 mg/ml and magnesium concentrations of 5–500 m*M*, while Härd and Kearns [10] have done so for 90 base-pair DNA fragments in solutions where DNA concentration ranged from 7.5–17 mg/ml and magnesium concentration ranged from 10–50 mM.

The suitability of the equations of state is demonstrated by calculation of the clustering functions that they imply. For the 0.1 *M* $MgCl_2$ dialysate the log of the quantity $(kT/M_2)(d\Pi/dc_2)^{-1}$ was calculated according to SPT using the radius from Table 2. As seen in Fig. 2a, there is a close agreement between the theoretical and the experimental clustering functions. This is also found for the 0.5 and 1.0 *M* $MgCl_2$ dialysates. In the low-salt case the theoretical clustering function takes the form [1]:

$$\frac{kT}{M_2}\left(\frac{d\Pi}{dc_2}\right)^{-1} = N_{Av}\left(1 + 2B_2 + M_2c_2 + 3B_3M_2c_2^2\right)^{-1}, \qquad (5)$$

where B_3 is set to zero for the 10 and 15 m*M* $MgCl_2$ samples. Correspondence of eq. (5) to the experimental clustering function for the 15 m*M* $MgCl_2$ dialysate is shown in Fig. 2b. Close correspondence is also found for the 1 and 10 m*M* $MgCl_2$ dialysates.

The critical parameters for the ordering phase transition are also presented in Table 2. The critical DNA concentration, c_{crit}, defined as the largest DNA concentration in the isotropic phase, can be expressed as a volume fraction occupied by effective solute particles, which for spherocylinders is [1]:

$$\phi_{eff} = \rho_{eff}V_{eff} = \frac{c_{crit}}{M_2}\pi N_{Av}a^2\left(\frac{3.4\cdot 10^{-8}M_2}{M_{bp}} + \tfrac{4}{3}a\right), \qquad (6)$$

where V_{eff} is the volume of an effective solute particle.

Because M_2 enters eq. (6) as M_2^{-1} (in relating mass concentration to number density) and as M_2 (to determine particle length) the errors in ϕ_{eff} due to uncertainty in M_2 are partly canceled (the second term between brackets in eq. 6 is negligible compared to the first). Consequently, the error of ϕ_{eff} is typically less than 5%. The physically impossible values of ϕ_{eff} for the 1 and 15 m*M* dialysates are further indications that the hard-core approximation is no longer valid for solutions equilibrated with 1–15 m*M* $MgCl_2$. These effective radii are only significant in terms of the energy of interaction for molecules this far apart. The effective critical volume fractions and corresponding effective axial ratios for the 0.1 *M*, 0.5 *M*, and 1.0 *M* $MgCl_2$ dialysates are in approxi-

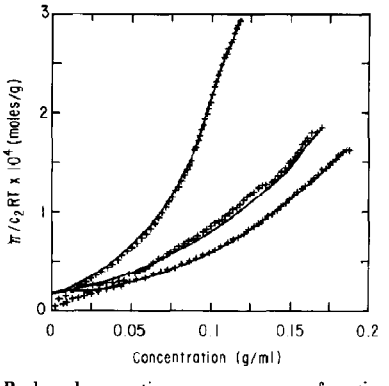

Fig. 4. Reduced osmotic pressure as a function of DNA concentration for (clockwise) 0.2 *M*, 0.5 *M*, and 1.0 *M* CsCl dialysates (the 1.5 *M* CsCl function was omitted for clarity). Experimental points are indicated by (+) and the solid curves were drawn according to SPT.

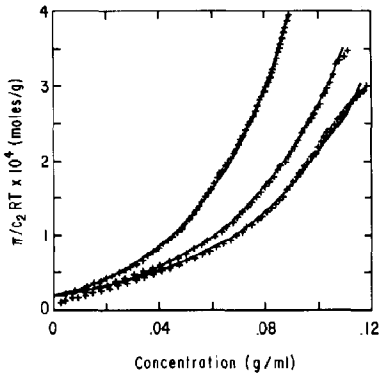

Fig. 5. Reduced osmotic pressure as a function of DNA concentration for (clockwise) 0.2 *M* LiCl, 0.2 *M* RbCl, and 0.2 *M* CsCl dialysates. Experimental points are indicated by (+) and the solid curves were drawn according to SPT.

mate agreement with theoretical predictions [16,24–26].

3.2 LiCl, RbCl and CsCl dialysates

The reduced osmotic pressure is plotted as a function of DNA concentration up to c_{crit} for DNA solutions dialyzed against 0.2–1.5 *M* CsCl in Fig. 4 and for solutions dialyzed against 0.2 *M* LiCl, 0.2 *M* RbCl, and 0.2 *M* CsCl in Fig. 5. The upward curvature, indicative of large contributions of many-body interactions to the pressure [16] increases with decreasing CsCl concentration and also as the counterion is changed from Cs^+ to Rb^+ to Li^+ when the ionic strength is 0.2.

A best fit of the SPT function to the experimental reduced osmotic pressure was again made by adjusting the molecular weight and hard-core radius independently to a minimum χ^2, while maintaining the relations stated in eq. (2). Close correspondence between theory and experiment is shown in Fig. 4 for the CsCl dialysates and in Fig. 5 for the 0.2 *M* alkali metal–chloride salt dialysates. Values for the hard-core radii corresponding to the best fits are presented in Table 3. They confirm the qualitative observations made of the experimental reduced osmotic pressure. Increased CsCl concentration results in greater charge screening between DNA helices represented by a diminishing hard-core radius. The hard-core radii for the 0.2 *M* alkali metal–chloride salt dialysates indicate that charge screening increases in the sequence $Li^+ < Rb^+ < Cs^+$. Hydration forces deriving from the orientation of water molecules at the DNA surface contribute significant repulsion between close helices, but the measurements of Rau et al. [12] show the repulsion to increase from Li^+ to Cs^+. Our sequence appears instead to follow the hydration number of the cation, which decreases with increasing crystal radius, and suggests that hydration forces between helices are less significant at this range of separation.

The molecular weights obtained from the fits by SPT are not uniform and are on the order of one-half the average value obtained from gel electrophoresis. Molecular weight relates the particle concentration to mass concentration as measured

Table 3

Effective radii, molecular weights, asymmetry ratios and critical parameters for LiCl, RbCl and CsCl dialysates

[Salt] [a]	a [b] (Å)	M_2 [c] ($\times 10^4$ g mol^{-1})	l/a [d]	$(\Pi/c_2RT)_{crit}$ ($\times 10^4$ mol g^{-1})	c_{crit} (g ml^{-1})	ϕ_{crit}
0.200 *M* LiCl	22.7	5.36	14.7	3.98	0.0895	0.469
0.200 *M* RbCl	22.2	5.91	13.5	3.45	0.111	0.499
0.200 *M* CsCl	21.6	5.73	12.2	2.93	0.118	0.504
0.500 *M* CsCl	16.0	5.29	14.7	1.82	0.170	0.350
1.00 *M* CsCl	15.1	9.26	25.6	1.60	0.187	0.328
1.50 *M* CsCl	14.4	7.14	21.1	1.52	0.189	0.306

[a] Dialysate salt concentration.
[b] DNA hard-core radii.
[c] DNA molecular weight.
[d] Asymmetry ratio.

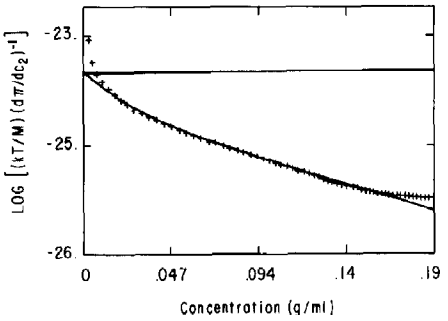

Fig. 6. Log of the clustering function versus DNA concentration for the 1.0 *M* CsCl dialysate. Points (+) were calculated from the experimental data and the solid curve was drawn according to SPT.

and also determines the particle length. The hard-core radius is not very sensitive to the variation in molecular weight; doubling M_2 changes the hard-core radius by about 5%. Also, a smaller molecular weight for the isotropic phase than for the original solution is consistent with the theoretical prediction that the longer particles of a polydisperse system of rods will segregate into the anisotropic phase [18–21].

The close agreement between the experimental clustering function and the function calculated from SPT parameters is shown in Fig. 6 for the 0.5 *M* CsCl dialysate. Representative of all samples, the function decreases monotonically indicating that the net interaction between helices is exclusively repulsive. Exclusively repulsive net interactions are also found for the other alkali metal–chloride salt dialysates.

The critical parameters for the ordering transition for the LiCl, RbCl, and CsCl dialysates are presented in Table 3. The effective volume fractions, computed using eq. (6), and the effective axial ratios are in good agreement with theoretical predictions [1,24,26].

4. Conclusions

Magnesium ion screens electrostatic repulsion between DNA helices much more strongly than univalent counterions—the effective helical radius at 0.1 *M* MgCl (10.5 Å) is less than that found at 2.0 *M* NaCl (11.7 Å) [1]. In the range of 1 m*M*–1.0 *M* $MgCl_2$, the minimum effective radius was found to correspond to a dialysate concentration of 0.1 *M* $MgCl_2$ in agreement with an earlier result (Lerman and Wang, unpublished) that PEO-induced DNA condensation requires lower PEO concentration at 0.1 *M* $MgCl_2$ than at either higher or lower magnesium concentration. Also, in the range of 0.1–1.0 *M* $MgCl_2$, adjacent DNA helices appear to share common Mg^{2+} counterions in agreement with the studies of Auer et al. [22], Fried and Bloomfield [9], and Härd and Kearns [10]. In the case of univalent counterions the degree of electrostatic screening increases with the crystal radius of the counterion, not with the counterion's hydration number, suggesting that hydration pressure is not the dominant force between non-parallel DNA helices at this range of separation.

Acknowledgements

This work as supported by Grant DMR 8515519 from the National Science Foundation.

References

1 A.A. Brian, H.L. Frisch and L.S. Lerman, Biopolymers 20 (1980) 1305.
2 S. Trohalaki, H.L. Frisch, A.A. Brian and L.S. Lerman, Biophys. J. 45 (1984) 777.
3 H. Reiss, H.L. Frisch and J.L. Lebowitz, J. Chem. Phys. 31 (1959) 369.
4 M.A. Cotter and D.A. Martire, J. Chem. Phys. 52 (1970) 1909.
5 M. LeBrett and B.H. Zimm, Biopolymers 23 (1984) 271.
6 G.S. Manning, Quart. Rev. Biophys. 11 (1978) 179.
7 J.A. Schellman and D. Stigter, Biopolymers 16 (1977) 1415.
8 D. Stigter, J. Phys. Chem. 82 (1978) 1603.
9 M.G. Fried and V.A. Bloomfield, Biopolymers 23 (1984) 2141.
10 T. Härd and D.R. Kearns, Biopolymers 25 (1986) 1519.
11 M. Mandelkern, N. Dattagupta and D.M. Crothers, Proc. Natl. Acad. Sci. U.S.A. 78 (1981) 4294.
12 D.C. Rau, B. Lee and V.A. Parsegian, Proc. Natl. Acad. Sci. U.S.A. 81 (1984) 2621.
13 R.L. Rill, P.R. Hillard Jr. and G.C. Levy, J. Biol. Chem. 258 (1983) 250.

14 A. Weissberger, Physical methods of organic chemistry (Wiley-Interscience, New York, NY, 1945).
15 G. Cohen and H. Eisenberg, Biopolymers 6 (1968) 1077.
16 B.H. Zimm, J. Chem. Phys. 14 (1946) 164.
17 L. Onsager, Annu. N.Y. Acad. Sci. 51 (1949) 627.
18 A. Abe and P.J. Flory, Macromolecules 11 (1978) 119.
19 P.J. Flory and A. Abe, Macromolecules 11 (1978) 1119.
20 P.J. Flory and R.S. Frost, Macromolecules 11 (1978) 1126.
21 R.S. Frost and P.J. Flory, Macromolecules 11 (1978) 1134.
22 C. Auer, L.S. Lerman and S. Wang, unpublished as reported in: C. Auer, Ph.D. Dissertation, Vanderbilt University (1976).
23 L.S. Lerman, Proc. Natl. Acad. Sci. U.S.A. 68 (1971) 1126.
24 P.J. Flory, Proc. R. Soc. Lond. Ser. A 234 (1956) 73.
25 A. Isihara, J. Chem. Phys. 19 (1951) 1142.
26 G. Lasher, J. Chem. Phys. 53 (1970) 4141.